Journal of Aerosol Science 166 (2022) 106067

Contents lists available at ScienceDirect

Journal of Aerosol Science

journal homepage: www.elsevier.com/locate/jaerosci

Primary aerosol emissions from lignocellulosic biomass and major constituents under well-defined pyrolysis conditions

Luke P. McLaughlin, Erica L. Belmont *

Department of Mechanical Engineering, The University of Wyoming, Laramie, WY, United States

ARTICLE INFO

Keywords:
Aerosol emissions
Burn phase
Biomass
Lignocellulosic composition
Macro-TGA

ABSTRACT

Near-source aerosol emissions from biomass burning are challenging to model and predict because of the complexity of the feedstocks and the evolved species, as well as the potential variability in local conditions. This study investigated and characterized near-source emissions from biomass and biomass constituent pyrolysis under well-defined conditions, providing data for validation of aerosol formation models and sub-models, and tested a hypothesis that near-source aerosol emissions from biomass can be predicted through a summative model approach based on constituent emissions and lignocellulosic biomass composition. Aerosol emission factors, concentrations, sizes, and volatility were assessed during highly repeatable lignocellulosic biomass and constituent pyrolysis experiments using a macro-TGA. Lignin and cellulose were found to produce significantly more and larger pyrolysis aerosol emissions than hemicellulose, and lignin produced aerosols with lower volatility than those from hemicellulose and cellulose. Lignocellulosic composition was investigated for its influence on primary aerosol emissions from biomass pyrolysis, including contributions to aerosol quantity, size, and volatility, through two approaches. First, the superposition model was tested using experimental aerosol measurements from individual constituents. Second, a simulated pine sample was produced by mixing constituents in the proportions in which they are present in pine, and aerosol emissions from pyrolysis of this sample were experimentally measured. Simulated aerosol emissions from superposition modeling and mixed-constituent-derived "pine" were compared to elucidate synergistic constituent influences on aerosol formation, and both results were found to predict pinewood aerosol emissions well. Conclusions regarding the successes and failures of the superposition model in predicting primary biomass aerosol emissions under similar conditions were drawn. Lastly, the influence of combustion on the biomass aerosol emissions under the conditions studied in this work was characterized to highlight the applicability and limitations of the pyrolysis results presented in this work to near-source aerosols formed under oxidative conditions.

1. Introduction

Complex burning parameters that are difficult to measure and predict ultimately dictate the primary physical, chemical, and optical properties of aerosols produced during biomass burning (BB) (Jolleys et al., 2014; Nielsen et al., 2017; Yang et al., 2021). Burning parameters are extremely dynamic in real burning events and include, but are not limited to, fuel composition, fuel moisture, oxygen

* Corresponding author. 1000 E. University Ave, Laramie, WY, 82071, United States.
E-mail address: ebelmont@uwyo.edu (E.L. Belmont).

https://doi.org/10.1016/j.jaerosci.2022.106067
Received 20 March 2022; Received in revised form 23 July 2022; Accepted 31 July 2022
Available online 14 August 2022

availability, burn phase (pre-ignition, flaming, smoldering), and dilution conditions (Collier et al., 2016; Fachinger, Drewnick, Gieré, & Borrmann, 2017; May et al., 2014; McLaughlin & Belmont, 2021a; Sakamoto, Laing, Stevens, Jaffe, & Pierce, 2016; Van Zyl et al., 2019). Furthermore, open BB emissions, where burning conditions are extremely dynamic and stochastic, are distinctly different from those of contained BB where burning is more controlled (Bond et al., 2004). Due to the overall complexity of BB and numerous influential burn parameters that influence the produced emissions, it is not feasible for a single investigation, nor series of investigations, to isolate and elucidate effects of all the physical and chemical phenomena influencing primary BB aerosol formation. Thus, a need for targeted studies that focus on specific influential burn parameters and contribute well-defined aerosol emission data sets has been identified in the literature (Jolleys et al., 2014). The study presented in this paper relates the aerosol emissions of individual lignocellulosic biomass constituents – cellulose, hemicellulose, and lignin – to those of real biomass under well-defined and highly repeatable pyrolysis conditions, and contributes well-defined data sets of primary biomass and constituent aerosol emissions as validation targets for complex aerosol formation models, submodels, and other experimental data.

Pyrolysis is the thermal degradation of fuel when heated, and the process produces a solid char, gases, and condensable tars or liquids (Evans & Milne, 1987; Shafizadeh, 1982). The formation of pyrolysis products has been well-explored in the literature and a clear and detailed overview is presented by Fawaz et al. (Fawaz, Avery, Onasch, Williams, & Bond, 2021). In brief, gaseous and condensable products of pyrolysis are released from the solid fuel, and condensable liquids are then either broken down to smaller species at higher temperatures, consumed and/or chemically altered by subsequent gas-phase oxidation, or some fraction condenses to form particles (Fawaz et al., 2021; Morf, Hasler, & Nussbaumer, 2002; Zhang, Obrist, Zielinska, & Gertler, 2013). Although pure pyrolysis in 0 vol% O_2 may not occur in naturally occurring BB events, experimentation in inert environments – such as was conducted in the study presented in this paper – can provide fundamental insights into primary organic aerosol formation by removing complex influences of combustion chemistry on fuel consumption and conversion of particle precursor species to particles.

Among the complicating factors in primary aerosol formation is fuel composition. Biomass types are understood to vary broadly in lignocellulosic composition (Cai et al., 2017), and lignocellulosic biomass constituents are understood to form unique devolatilization products (Fitzpatrick et al., 2007; Mitchell et al., 2016; Orasche et al., 2013; Reid, Koppmann, Eck, & Eleuterio, 2005). Lignin is an aromatic polymer that produces phenolic compounds and participates in guaiacyl unit formation, whereas cellulose and hemicellulose produce anhydrous sugars and participate in furfural and furan formation (Fitzpatrick et al., 2007; Mitchell et al., 2016; Orasche et al., 2013). In addition to lignocellulosic content, biomass contains proteins, extractives, and inorganic content in a broad range of mass fractions (Vassilev, Vassileva, Song, Li, & Feng, 2017), and this content can contribute to aerosol formation and fine particulate emissions during combustion (May et al., 2014; Yang et al., 2021). Lignocellulosic composition has been shown to determine pyrolysis behavior in thermally thin fuels, defined as fuels in which heat is transferred throughout a particle almost instantly (Grønli, Várhegyi, & Di Blasi, 2002). Furthermore, the proportions of pyrolysis char and condensable liquid production from thermally thick wood have been shown to be strongly dependent on holocellulose (total of cellulose and hemicellulose) and lignin composition (Di Blasi, Branca, Santoro, & Gonzalez Hernandez, 2001). Di Blasi et al. (Di Blasi et al., 2001) showed that fuels with large holocellulose composition compared to lignin composition produce large quantities of condensable liquids, and fuels with large lignin content tend to produce large char quantities. These findings strongly suggest that lignocellulosic biomass composition significantly influences the primary organic aerosols formed from biomass pyrolysis, as condensable liquids or tars are understood to form particles following ejection from the fuel during pyrolysis (Zhang et al., 2013).

The development of a complex aerosol emission prediction model which accurately captures all of the influences of biomass burning conditions will require well-defined data sets to validate submodels that account for factors such as biomass composition. This study contributes well-defined and unique data sets of primary aerosol emissions from pyrolysis of pinewood biomass as well as individual lignocellulosic constituents under thoroughly characterized and readily modeled conditions. Additionally, the work evaluates a simple superposition model to test a hypothesis that primary biomass pyrolysis aerosol emissions can be predicted from lignocellulosic composition and the aerosol emissions of the three major constituents of lignocellulosic biomass when those constituents are exposed to the same conditions as the biomass itself. Biomass and constituent samples were pyrolyzed using a macro-scale thermogravimetric analyzer (macro-TGA), and aerosol concentrations, emission factors, median diameters, and volatility were determined using a cascade impactor and thermodenuder (TD). The superposition model tested in this work was developed in preceding works (McLaughlin & Belmont, 2021a; 2021b), and the simplified approach to BB aerosol prediction under well-controlled conditions is the first of its kind. Model-predicted aerosol emissions were compared to those of biomass, as well as experimental measurements of a simulated pine sample produced by mixing constituents in the proportions in which they are present in pine. Model and mixed constituent "pine" results were analyzed to assess the hypothesis that primary biomass pyrolysis aerosol emissions can be predicted by lignocellulosic composition alone when exposed to the same conditions, and successes and failures of the model under the conditions studied in this work were analyzed. The data presented in this study contribute novel insights into the influences that individual lignocellulosic constituents have on the quantity, size, and volatility of aerosols formed during biomass pyrolysis, as well as synergistic effects between constituents that influence aerosol formation. The biomass and constituent aerosol data presented here represent very fresh biomass pyrolysis aerosols, thus the data are not intended for comparison with atmospheric aerosol models. Rather, the data provide targets for development of current and future state-of-the-art aerosol formation models, submodels, and other experimental data which incorporate additional physical, chemical, and transport phenomena that influence biomass aerosol formation.

2. Methods and materials

2.1. Lignocellulosic biomass and constituent samples

Lodgepole pinewood and the major lignocellulosic biomass constituents – cellulose, hemicellulose, and lignin – were chosen for investigation in this study. The pinewood was sourced from the Medicine Bow National Forest, ground into wood chips using an industrial blender, dried at 100 °C for 24 h, and stored in a desiccator until use in experiments. Wood chips were explored in this work, compared to pulverized wood in preceding works (McLaughlin & Belmont, 2021a; 2021b), to investigate the superposition hypothesis using fuel that is representative of litter fuel that burns in real BB events. The average wood chip width and height were 2.6 ± 1.1 mm and 24.3 ± 9.6 mm, respectively, giving an average aspect ratio of 1:9.3 with a Biot number range of 0.05–0.09. Cellulose, hemicellulose, and lignin were investigated using Avicel (Sigma Aldrich, PH-101), xylan (Megazyme, from Beechwood), and Kraft lignin with a 97% dry lignin content (Storaenso, from pine and Nordic spruce), respectively. An additional sample was created by mixing the representative individual constituent samples according to their respective mass fractions in the pinewood investigated in this work, and this sample is referred to as "mixed-pine". The mixed-pine sample was created to elucidate any synergistic influences of biomass constituents on fuel devolatilization and aerosol formation that are not represented by the modeled superposition of individual constituent results as evaluated in this work. The individual and mixed-constituent samples, having a powder form, were compacted into discs using a twenty-ton hydraulic press and then broken into chips to match the dimensions of the pinewood chips. Both the pinewood and constituent samples were considered dry as each sample had a moisture content of less than 4 wt% at the time of experimentation.

Moisture content, volatile content (VC), fixed carbon content (FC), and ash content (AC) were characterized for the pinewood, individual constituents, and mixed-pine using the KAR procedure (López-García et al., 2013), which is a slightly modified ASTM D7582 proximate analysis method. The KAR procedure results are presented on a dry basis in Table 1. The cellulose, hemicellulose, lignin, and other contents of the pinewood sample were characterized by the National Renewable Energy Laboratory (NREL) in Golden, CO, and the major constituent results are also shown in Table 1. Galactan, arabinan, and mannan were added to the hemicellulose mass fraction. The proteins, extractives, and inorganic content made up the remaining 15.2 wt%, and their role in aerosol formation was not included in the modeling of this work, as the hypothesis tested in this work was that primary biomass pyrolysis emissions can be predicted from the contributions of the three major constituents – hemicellulose, cellulose, and lignin – alone. Nevertheless, the successes and failures of the simplified modeling approach in this work can lend insights into potential influences of the outstanding biomass content on pyrolysis aerosols, and the technique presented in this work can readily be applied in future work to incorporate biomass inorganics and other contents and evaluate their influences on particle precursor species and aerosol formation.

2.2. Experimental platform

Biomass and constituent aerosol concentrations, emission factors, size, and volatility were investigated in this work by performing pyrolysis experiments using a well-characterized macro-TGA platform. The TGA approach to biomass pyrolysis aerosol characterization was developed in preceding work using a micro-TGA (McLaughlin & Belmont, 2021a; 2021b). This work increased the investigation scale from the micro to macro scale, concomitantly altering aerosol residence time in the TGA furnace, the number of dilution stages, and fuel preparation. The influence of scale change on biomass pyrolysis aerosol emissions can be found in work by McLaughlin (McLaughlin, 2022). A schematic of the experimental setup used in this work is shown in Fig. 1.

The macro-TGA consists of a Carbolite KVT1200 vertical split tube furnace surrounding a 1.22 m tall and 0.19 m inner diameter quartz tube, and a custom load cell frame. The quartz tube is sealed at the bottom with a stainless-steel cap to control gas flow through the furnace. The load cell frame consists of an RSP1 Single Point Load Cell by Loadstar Sensors for real-time mass measurements, a hang-down wire to suspend inside the quartz tube a custom sample pan constructed of ZIRCAR Ceramics MICROSIL insulation, and a 0.61 m K-type thermocouple for real-time gas environment temperature measurements approximately 0.18 m above the sample. The real-time mass measurements were corrected for buoyancy influences using data acquired with an empty sample pan exposed to the same heating conditions. The corrected real-time mass measurements were then utilized to determine fuel mass loss rates on relative and absolute bases, defined here as the change in percentage of initial fuel mass with time (relative mass loss rate, RMLR) and change in absolute mass of fuel with test time (absolute mass loss rate, AMLR), respectively. The load cell is protected from the high-temperature gas exiting the furnace by a 0.05 m thick ZIRCAR Ceramics MICROSIL insulation plate (not shown in Fig. 1 for

Table 1
Dry-basis proximate and constituent analyses of the pinewood, major lignocellulosic biomass constituents, and mixed-constituent sample (mixed-pine). All results are given in wt%, and VC≡volatile content, FC≡fixed carbon content, and AC≡ash content. Constituent analysis for pinewood was performed by NREL.

	VC	FC	AC	Lignin	Cellulose	Hemicellulose
Pinewood	85.6 ± 1.1	11.1 ± 1.1	3.3 ± 0.3	28.3	35.8	20.7
Cellulose	94.8 ± 0.2	4.5 ± 0.3	0.7 ± 0.2	n/a	100	n/a
Hemicellulose	83.2 ± 0.5	15.6 ± 0.4	1.3 ± 0.1	n/a	n/a	100
Lignin	64.7 ± 0.7	33.7 ± 1.2	1.6 ± 0.5	100	n/a	n/a
Mixed-Pine	82.9 ± 0.9	16.5 ± 0.8	0.6 ± 0.1	28.3	35.8	20.7

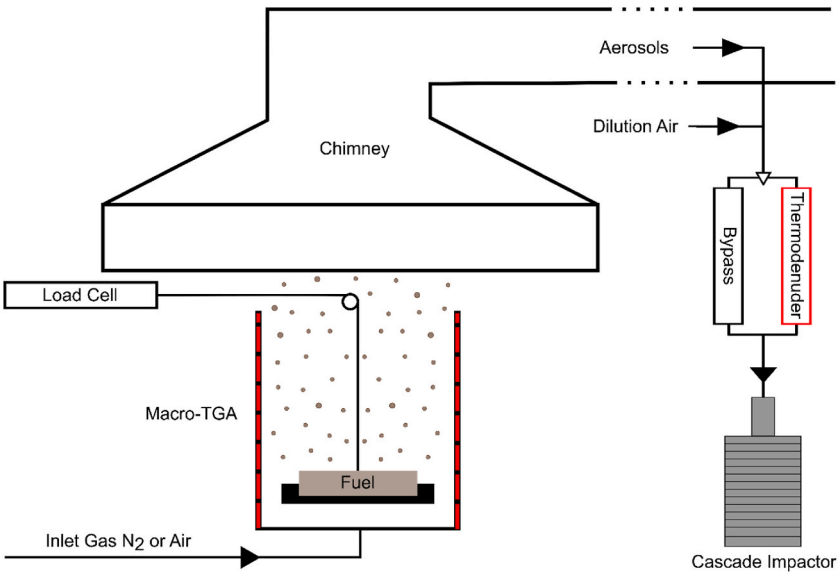

Fig. 1. Schematic of the experimental platform for pyrolysis, including a macro-TGA for mass loss measurement during feedstock conversion and a chimney for aerosol sampling, as well as a particle impactor for aerosol characterization.

simplicity) and a protective acrylic box that is purged with dry lab air.

Ultra-high purity nitrogen (N_2, 99.999%) flowed through the quartz tube and over the sample at a flow rate of 40 SLPM (standard liters per minute at 273 K and 1 atm) during pyrolysis. All of the samples investigated in this study were heated at an average heating rate of 25 °C·min^{-1} from 22 °C to 700 °C and held isothermal until the samples were fully pyrolyzed, as indicated by a constant sample mass, and aerosol formation ceased. The starting fuel mass for experiments was 10 g for each fuel type, except for the mixed-pine which had a starting fuel mass of 8.5 g to exclude the 15.2 wt% of protein, extractive, and inorganic content of the pinewood which were not incorporated into the modeling of this work.

Emissions produced during pyrolysis exited the furnace and were drawn into a chimney along with ambient lab air. The chimney has a total flow rate of 29.7 m^3·min^{-1} which resulted in a chimney dilution ratio, defined as the ratio of gas flow rate from the macro-TGA to additional dilution air flow rate entrained by the chimney, of approximately 1:742. Additionally, a normalized dilution ratio was defined as the ratio of gas flow rate from the macro-TGA normalized by fuel mass to additional dilution air flow rate entrained by the chimney and was approximately 1 SLPM·g^{-1}:7430 SLPM. A fraction of the diluted emissions was then sampled from the center of the chimney cross-section and at a distance 3.1 m downstream of the chimney entrance using a rotary vane vacuum pump and at a rate of 2.7 SLPM. The sampled emissions were diluted once more with 4.0 SLPM of dry lab air to further reduce the particle concentration for aerosol detection, resulting in a secondary dilution ratio of 1:1.7 and a total flow rate of 6.7 SLPM for analysis. The mixture was then drawn through a stainless steel bypass line (BP) or Dekati Thermodenuder TD3 (TD) before detection by a 14-stage Dekati High-Temperature Electrical Low-Pressure Impactor (HT-ELPI) for real-time aerosol size and number measurements. Avoidance of pyrolysis product condensation in sample lines was obtained through substantial dilution of pyrolysis products, and success was assessed through the excellent repeatability of experiments over many hours of system operation, as reflected in the measurement uncertainty presented in this work. Uncertainty characterization is discussed in Section 2.3.

The residence time of the aerosols in the furnace was approximately 8.3 s and the residence time of the aerosols in the system from exiting the furnace to detection was approximately 6.0 s. The residence time of aerosols in the heated section of the TD ranged from 0.5 to 0.9 s between TD operating temperatures of 75–300 °C tested in this work. Thermodenuder heated section residence time, input aerosol size distribution, and aerosol loading have been shown to influence aerosol evaporation equilibrium (An, Pathak, Lee, & Pandis, 2007; Faulhaber et al., 2009; Huffman, Docherty, Aiken, et al., 2009; Huffman, Docherty, Mohr, et al., 2009), and thus these factors must be considered when comparing the aerosol volatility measurements presented here to those from other studies.

2.3. Experimental test overview

The pinewood, individual lignocellulosic biomass constituents, and mixed constituent sample (mixed-pine) were investigated in 100% N_2 pyrolysis experiments. Aerosol emissions were determined for pinewood while operating the system with the bypass and the TD at temperatures of 75, 150, 225, and 300 °C. Individual constituent samples and the mixed-pine were tested while operating the system with the bypass and the TD at temperatures of 150 and 300 °C. Each test configuration was tested at least twice to obtain trial-to-trial measurement uncertainty using Student's t-test with a 95% confidence interval. The raw signals of each impactor collection stage were analyzed for signal-to-noise ratio (SNR) during their peak signal period in each experiment, and impactor stages with an SNR of less than one were removed from the final analysis (McLaughlin & Belmont, 2021a; 2021b). Comprehensive data sets that

include data for each impactor stage and denote removed stages are presented in the Supplemental Material. Furthermore, the validity of the aerosol measurements was supported by performing several checks, including zero-air checks, blank sample runs, and HEPA filter tests, to ensure that the aerosol measurements were not artifacts of the measurement technique. Additional information regarding the checks can be found in McLaughlin & Belmont (McLaughlin & Belmont, 2021b).

2.4. Emission factors

Real-time HT-ELPI aerosol number concentration measurements and macro-TGA load cell mass loss measurements were utilized to calculate the number and mass emission factors for each impactor collection stage over a given time period. The time-resolved particle number concentration of each impactor stage ($N_i(t)$) was integrated over a time period (δt), multiplied by the volumetric flow rate through the impactor ($\dot{V}$), and divided by the fuel mass consumed over the time period (m_{fuel}) to determine the corresponding number emission factor ($EF_{N,i}$). The total number emission factor ($EF_{N,tot}$) was determined by summing the size-resolved number emission factor of each impactor stage as shown in Eqn. 1

$$EF_{N,tot} = \sum_{i=1}^{n} E_{N,i} = \sum_{i=1}^{n} \frac{\dot{V} \cdot \int_{\delta t} N_i(t) \cdot dt}{m_{fuel}} \tag{1}$$

where n is the number of included stages in the HT-ELPI. The mass emission factor of each impactor stage ($EF_{M,i}$) was determined from the corresponding number emission factor, and total emission factor ($EF_{M,\ tot}$) was determined by

$$EF_{M,\ tot} = \sum_{i=1}^{n} EF_{M,i} = \sum_{i=1}^{n} \rho \cdot V_i \cdot EF_{N,i} \tag{2}$$

where ρ is the particle density, assumed to be 1 g cm^{-3} because the aerodynamic diameter (D_i) was used to determine mass following the operating principle of the HT-ELPI, and V_i is the particle volume calculated from D_i. Number and mass emission factors were determined for periods corresponding to the full pyrolysis tests.

2.5. Aerosol volatility

Aerosol volatility was assessed in this work as the mass fraction remaining (MFR) of the aerosol stream in the particle phase after passing through the TD, as compared to the bypass, at a given TD temperature. This technique produces thermograms that have a value of unity at room temperature and decrease with increased TD temperature. MFR as a function of TD temperature was determined for each sample by

$$MFR(T_{TD}) = \frac{EF_{M,tot,TD}(T_{TD})}{EF_{M,tot,BP}} \tag{3}$$

where $EF_{M,tot,BP}$ and $EF_{M,tot,TD}$ are total mass emissions factors derived from the system operating with the bypass and TD, respectively, and with the TD operating at temperature T_{TD}.

2.6. Simulated aerosol emissions

Pinewood aerosol concentrations, emission factors, size, and volatility were simulated utilizing a previously developed superposition model for aerosol emission factor prediction based upon lignocellulosic biomass constituents and their mass fractions in the biomass (McLaughlin & Belmont, 2021a; 2021b). This model tests the hypothesis that primary biomass pyrolysis aerosol emissions can be predicted from lignocellulosic composition and constituent emissions when biomass and constituent emissions are measured under the same set of pyrolysis conditions. This model was previously developed and tested at a much smaller scale in preceding work (McLaughlin & Belmont, 2021a; 2021b). While the present work focuses on testing this model and hypothesis at larger scales and focusing on the three major lignocellulosic constituents of biomass, the successes and failures of this simplified modeling approach can provide new insights into influences of other potential contributing factors, such as biomass inorganic content, to the formation of organic aerosols, and the approach can be expanded to test these other influences in future work. Additionally, validation of a superposition model and the present hypothesis regarding major constituents in this work can guide and provide validation targets for more complex models and experiments that incorporate other physical, chemical, and transport phenomena affecting BB aerosol formation.

The superposition model predicts both size-resolved and total emission factors of biomass using experimental measurements from individual lignocellulosic biomass constituents and the constituent mass fractions in the biomass being modeled. In this work, the superimposed constituent pyrolysis results are referred to as “super-pine”, and the results were compared to pinewood and mixed constituent (mixed-pine) pyrolysis results. The mass fractions of the major lignocellulosic biomass constituents reported in Table 1 were used in combination with the measured pyrolysis emissions factors from each of the individual constituents to produce super-pine emission factors. The superposition formulas used to simulate the pinewood number ($EF_{N,\ sim}$) and mass ($EF_{M,\ sim}$) emission factors, both size-resolved and total, were

$$EF_{N,\ sim} = EF_{N,h} \cdot Y_h + EF_{N,c} \cdot Y_c + EF_{N,l} \cdot Y_l \quad (4)$$

$$EF_{M,\ sim} = EF_{M,h} \cdot Y_h + EF_{M,c} \cdot Y_c + EF_{M,l} \cdot Y_l \quad (5)$$

where Y_h, Y_c, and Y_l are the mass fractions of hemicellulose, cellulose, and lignin, respectively, determined for the pinewood, and $EF_{N,h}$, $EF_{N,c}$, $EF_{N,l}$, $EF_{M,h}$, $EF_{M,c}$, and $EF_{M,l}$ are the size-resolved or total number and mass emission factors, determined with either the bypass or TD, over the entire constituent pyrolysis experiments for hemicellulose, cellulose, and lignin.

In this work, the model was expanded from previous work to simulate time-resolved bypass number ($N(t)_{tot,\ sim}$) and mass concentrations ($M(t)_{tot,\ sim}$), as well as relative fuel mass loss rate ($RMLR(t)_{sim}$). The superposition equations are as follows

$$N(t)_{tot,\ sim} = N(t)_{tot,h} \cdot Y_h + N(t)_{tot,c} \cdot Y_c + N(t)_{tot,l} \cdot Y_l \quad (6)$$

$$M(t)_{tot,\ sim} = M(t)_{tot,h} \cdot Y_h + M(t)_{tot,c} \cdot Y_c + M(t)_{tot,l} \cdot Y_l \quad (7)$$

$$RMLR(t)_{sim} = RMLR(t)_h \cdot Y_h + RMLR(t)_c \cdot Y_c + RMLR(t)_l \cdot Y_l \quad (8)$$

where $N(t)_{tot,h}$, $N(t)_{tot,c}$, $N(t)_{tot,l}$, $M(t)_{tot,h}$, $M(t)_{tot,c}$, $M(t)_{tot,l}$, $RMLR(t)_h$, $RMLR(t)_c$, and $RMLR(t)_l$ are the time-resolved total bypass number concentrations, mass concentrations, and relative fuel mass loss rates measured during pyrolysis experiments for hemicellulose, cellulose, and lignin. The model was also further developed in this work to predict the volatility of simulated aerosol emissions using MFR, as determined by

$$MFR_{sim}(T_{TD}) = \frac{EF_{M,tot,\ sim,TD}(T_{TD})}{EF_{M,tot,sim,BP}} \quad (9)$$

where $EF_{M,tot,\ sim,BP}$ and $EF_{M,tot,\ sim,TD}$ are the simulated bypass and TD super-pine emission factors, respectively.

3. Results and discussion

3.1. Pinewood pyrolysis aerosol emissions

Time-resolved total aerosol number and mass concentrations are shown for pinewood pyrolysis in Fig. 2 to elucidate predominant test times and temperatures at which aerosol mass and number concentrations are elevated under the applied conditions. Results are shown for the bypass and each tested TD temperature (75, 150, 225, and 300 °C) to provide insight into the volatility of pinewood pyrolysis aerosols with test time. Additionally, a representative RMLR and representative gas environment temperature (T) are shown.

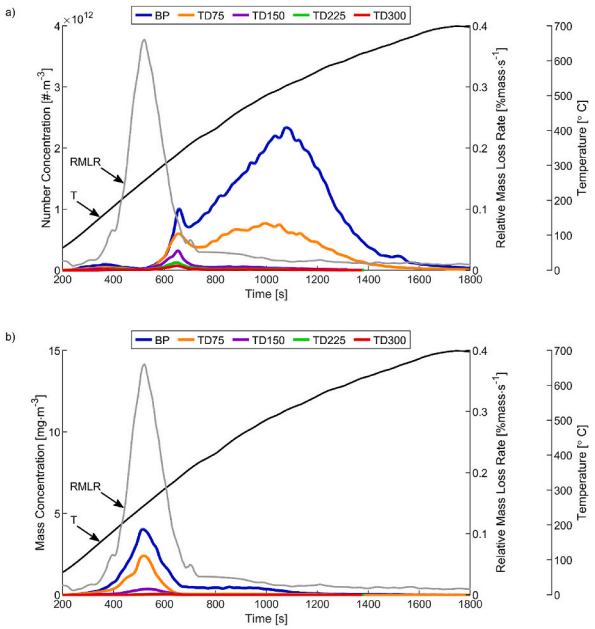

Fig. 2. Pinewood pyrolysis aerosol a) number and b) mass concentrations versus time, with emissions passed through either the bypass line (BP) or the thermodenuder (TD) over a range of TD temperatures (75, 150, 225, and 300 °C). Representative relative mass loss rate (RMLR) and gas environment temperature (T) are shown on the second and third y-axes, respectively.

Bypass number and mass concentrations are greater than those at each TD temperature due to the volatilization of an increasing fraction of aerosols at each progressively higher TD temperature.

The peak RMLR observed over the duration of the pinewood pyrolysis test was 0.38 %mass·s^{-1}. The peak RMLR aligned in time with the corresponding peak aerosol mass concentrations, and the result is attributed to an increased concentration of particle precursor species being ejected from the fuel at a high RMLR, increasing gas-to-particle conversion (May et al., 2013). This increased particle concentration formed early after the devolatilization event has been shown to increase aerosol coagulation and growth (Sakamoto et al., 2016), and heterogeneous condensation of particle precursor species is favorable in the presence of existing large particles (Jöller, Brunner, & Obernberger, 2005). The peak number concentration occurred after the peak RMLR, and this was attributed to aerosol formation proceeding predominantly by homogeneous nucleation at a low RMLR due to a lack of many pre-existing large particles for particle precursor species to condense upon (Jöller et al., 2005).

Size-resolved and total number and mass emission factors and median aerosol sizes were determined for pinewood pyrolysis using the bypass and TD, and the results are presented in the Supplemental Material. In each pyrolysis experiment, ultra-fine aerosols (<0.1 μm) dominated the number distribution while larger, accumulation-mode aerosols (0.1 μm $\leq D_i \leq$1 μm) dominated the mass distribution. The median bypass diameters corresponding to the midpoint of the aerosol distribution by number and mass, $D_{50,N,BP}$ and $D_{50,M,BP}$, were determined to be 0.016 ± 0.002 μm and 0.699 ± 0.002 μm. This result supports the finding by Iisa et al. (Iisa et al., 2019) that median pine-derived pyrolysis aerosols are <0.1 μm and 1 μm on a number and mass basis, respectively, following cooling. Total bypass number and mass emission factors, $EF_{N,tot,BP}$ and $EF_{M,tot,BP}$, were 7.7e13 ± 7.5e12 #·g^{-1} and 58.5 ± 4.6 mg·g^{-1} in the pyrolysis environment. $EF_{M,tot,BP}$ measured in this study is large compared to those typically reported for open pinewood burning, such as 11.2–33.5 g·kg^{-1} (Hays, Geron, Linna, Smith, & Schauer, 2002), 7.5–62.5 g·kg^{-1} (Grandesso, Gullett, Touati, & Tabor, 2011) and 7–77 g·kg^{-1} (Vose, Swank, Geron, & Major, 1996), where the upper limit of each cited range was associated with less efficient smoldering combustion. The large $EF_{M,tot,BP}$ in this work arises from the nature of the pyrolysis experiments performed, where volatile and semi-volatile particle precursor species which condense to form organic aerosol particles are not consumed or reduced due to oxidation and high combustion temperatures.

3.2. Time-resolved constituent aerosol concentrations

Time-resolved aerosol number and mass concentrations measured using the bypass sample line are shown for pyrolysis of each major lignocellulosic biomass constituent in Fig. 3 in order to elucidate unique trends of aerosol number and mass formation from each constituent sample. The constituent concentration data are shown along with a representative RMLR for each constituent and a representative gas environment temperature (T). The onset of devolatilization is observed first for hemicellulose, followed by cellulose, and then lignin. The peak RMLR was determined to be 0.33 %mass·s^{-1}, 0.32 %mass·s^{-1}, and 0.18 %mass·s^{-1} for hemicellulose, cellulose, and lignin, respectively. Lignin produced the largest peak number concentration whereas cellulose produced the largest peak mass concentration. Despite having a comparable RMLR to cellulose, hemicellulose produced the smallest peak mass concentration

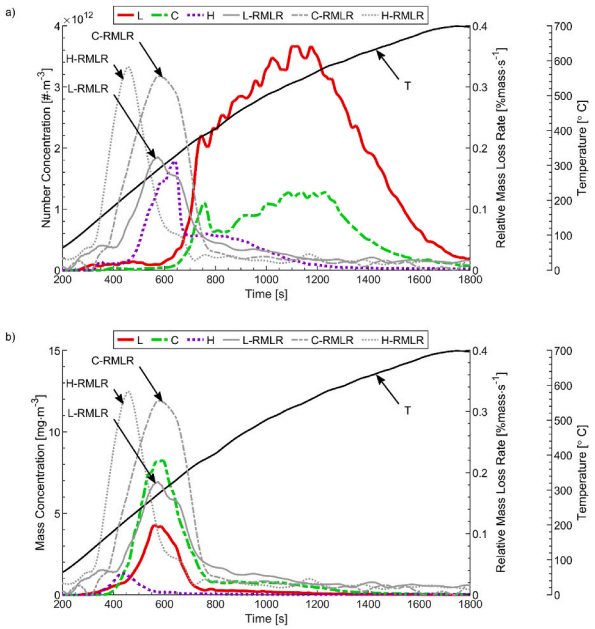

Fig. 3. Comparison of lignocellulosic biomass constituent-derived aerosol a) number and b) mass concentrations over pyrolysis time obtained using the bypass sample line. The relative mass loss rate (RMLR) is also shown for lignin (L) as L-RMLR, cellulose (C) as C-RMLR, and hemicellulose (H) as H-RMLR, along with a representative gas environment temperature (T).

compared to the other constituents, and this result is consistent with preceding work which showed negligible aerosol emission contributions from hemicellulose in biomass compared to contributions from cellulose and lignin (McLaughlin & Belmont, 2021a; 2021b). Similar to results for pinewood pyrolysis (Section 3.1), the peak mass concentration of each constituent corresponded in time with their respective peak RMLR while the peak number concentration occurred after their respective peak RMLR.

3.3. Constituent aerosol emission factors and median size

Size-resolved $EF_{N,BP}$ and $EF_{M,BP}$ were determined for hemicellulose, cellulose, and lignin over the duration of pyrolysis, and results are shown in Fig. 4. Aerosols with aerodynamic diameters greater than 2.0 μm did not meet the SNR criteria in this work and were therefore not included in the reported aerosol number and mass emission factors. Ultra-fine aerosols (<0.1 μm) dominated the number distribution whereas accumulation-mode aerosols (0.1 μm $\leq D_i \leq$ 1 μm) dominated the mass distribution. The median diameters corresponding to the midpoints of the aerosol distributions by number and mass, $D_{50,N,BP}$ and $D_{50,M,BP}$, are tabulated in Table 2. Cellulose produced the largest $D_{50,N,BP}$ and second-largest $D_{50,M,BP}$, whereas lignin produced the largest $D_{50,M,BP}$ and relatively small $D_{50,N,BP}$, and hemicellulose produced relatively small $D_{50,N,BP}$ and $D_{50,M,BP}$. $EF_{N,tot,BP}$ and $EF_{M,tot,BP}$ are also shown in Table 2 for each constituent. Lignin produced the largest $EF_{N,tot,BP}$ and the second-largest $EF_{M,tot,BP}$, while cellulose produced the second-largest $EF_{N,tot,BP}$ and the distinctly largest $EF_{M,tot,BP}$. Hemicellulose produced the smallest $EF_{N,tot,BP}$ and $EF_{M,tot,BP}$, similar to preceding works (McLaughlin & Belmont, 2021a; 2021b). These emission factor and median size results suggest that cellulose and lignin are expected to contribute major roles in aerosol formation from BB while hemicellulose will contribute less significantly. This finding aligns with work by Iisa et al. (Iisa et al., 2019) which showed that cellulose and lignin pyrolysis products, including anhydrous sugars and phenols, significantly contribute to biomass pyrolysis aerosol formation.

The constituent mass emissions align with the findings of Di Blasi et al. (Di Blasi et al., 2001) that large holocellulose composition (total of cellulose and hemicellulose) promotes the production of condensable liquids during pyrolysis, as $EF_{M,tot,BP}$ of holocellulose was 119.5 $mg{\cdot}g^{-1}$ compared to 44.3 $mg{\cdot}g^{-1}$ of lignin in this work. It is noted that 91% of holocellulose mass emissions were contributed to by cellulose. $EF_{M,tot,BP}$ of the constituents are observed to be large compared to values typically reported for biomass burning. These discrepancies are attributed to two phenomena. First, the pyrolysis experiments performed in this work do not include consumption or decomposition of particle precursor species via oxidation and high combustion temperatures, as was discussed for pinewood in Section 3.1. Second, the partial pressure of pyrolysis products from pure constituents having the same saturation pressure is far greater than those produced from biomass per unit mass of fuel, and increased concentrations of particle precursor species from biomass has been shown to increase gas-to-particle conversion (May et al., 2013).

3.4. Constituent pyrolysis aerosol volatility

The MFR of aerosols in the emissions stream at TD temperatures of 150 °C and 300 °C were determined for each lignocellulosic biomass constituent during pyrolysis in order to better understand their unique influences on the volatility of biomass-derived aerosol emissions, and results are shown in Fig. 5. Lignin-derived aerosols had a significantly greater MFR at 150 °C (0.225 ± 0.022) compared to hemicellulose-derived (0.061 ± 0.003) and cellulose-derived (0.021 ± 0.004) aerosols, which were nearly completely volatilized at 150 °C. At a TD temperature of 300 °C, each constituent had less than 3.5% of its bypass aerosol mass remaining. The constituent pyrolysis MFR results, although investigated at only two TD temperatures, suggest that particle precursor species derived from lignin pyrolysis decrease the volatility of biomass pyrolysis aerosols, while precursor species derived from cellulose and hemicellulose pyrolysis increase biomass-derived aerosol volatility. These findings invite additional investigation into the volatility of individual constituent pyrolysis products in future work.

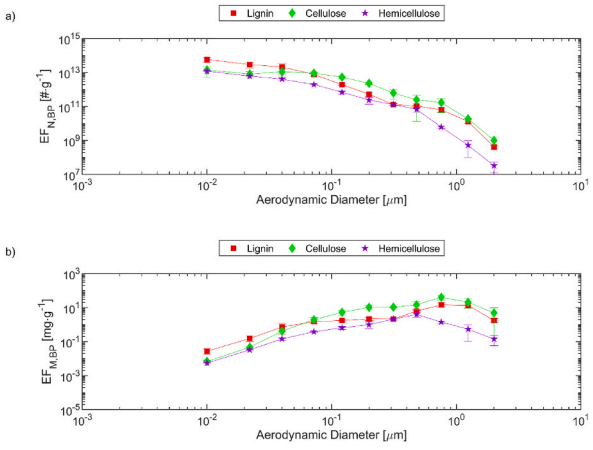

Fig. 4. Size-resolved a) number and b) mass aerosol emission factors determined for the pyrolysis of each lignocellulosic biomass constituent using the bypass (BP) sample line.

Table 2
Median aerosol number ($D_{50,N,BP}$) and mass ($D_{50,M,BP}$) diameters and total aerosol number ($EF_{N,tot,BP}$) and mass ($EF_{M,tot,BP}$) emission factors derived from pyrolysis of individual biomass constituents.

Constituent Pyrolysis	$D_{50,BP,N}$ [μm]			$D_{50,BP,M}$ [μm]			$EF_{N,tot}$ [#·g^{-1}]			$EF_{M,tot}$ [mg·g^{-1}]		
	Avg.		Dev.	Avg.		Dev.	Avg.		Dev.	Avg.		Dev.
Lignin	0.010	±	0.001	0.606	±	0.019	1.2E+14	±	2.5E+13	44.3	±	5.6
Cellulose	0.027	±	0.005	0.547	±	0.046	5.1E+13	±	1.1E+13	109.2	±	19.0
Hemicellulose	0.011	±	0.001	0.343	±	0.024	2.6E+13	±	8.6E+11	10.3	±	1.5

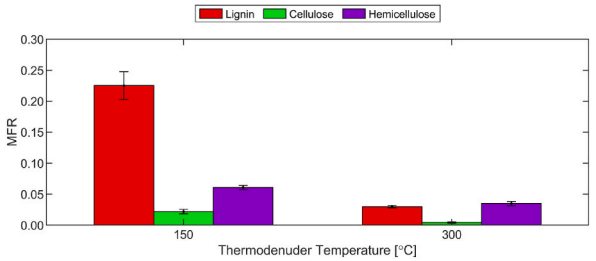

Fig. 5. Thermodenuded aerosol mass fraction remaining (MFR) from pyrolysis of lignin, cellulose, and hemicellulose. Two thermodenuder temperatures of 150 °C and 300 °C are shown.

3.5. Simulated time-resolved pinewood aerosol concentrations

The superposition model and hypothesis that fresh biomass pyrolysis aerosol emissions can be predicted from lignocellulosic composition and measured emissions from those constituents under the same pyrolysis conditions were first tested through the prediction of real-time aerosol number and mass concentrations using Eqns. (6) and (7). Superimposed constituent (super-pine) bypass results are compared to measurements of real pinewood and the mixed constituent sample (mixed-pine) in Fig. 6. A representative gas environment temperature (T) and representative RMLR for each measured and simulated sample are also shown. The peak RMLR was determined to be 0.38 %mass·s^{-1}, 0.17 %mass·s^{-1}, and 0.36 %mass·s^{-1} for pinewood, super-pine, and mixed-pine, respectively. The mixed-pine peak RMLR shows very good agreement with that of the pinewood, within 5%, whereas the super-pine showed agreement within 55%.

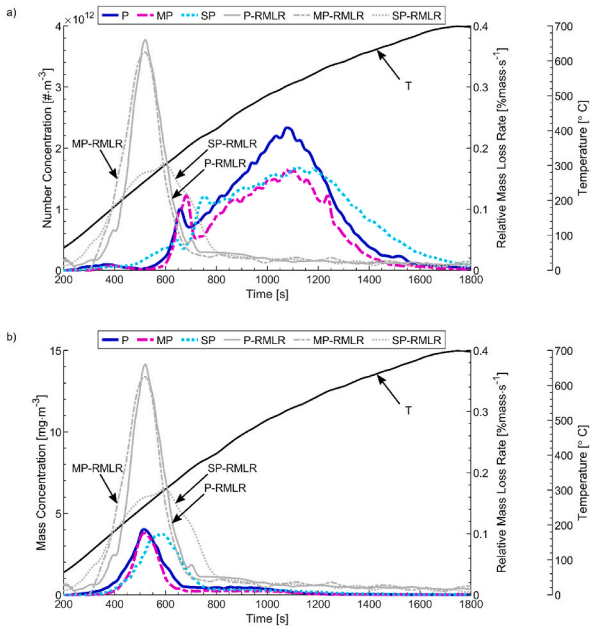

Fig. 6. Comparison of time-resolved super-pine (SP), mixed-pine (MP), and pinewood (P) pyrolysis-derived aerosol a) number concentration and b) mass concentration, with experimental measurements obtained using the bypass sample line. A representative relative mass loss rate (RMLR) is shown for each sample along with a representative gas environment temperature (T).

The shape, magnitude, and timing of the mixed-pine number and mass concentration profiles agree very well with those of the pinewood sample. Similar shape and magnitude agreement are observed between the super-pine and pinewood number and mass concentration profiles, but the peak super-pine mass and number concentrations are delayed by approximately 70 s compared to the pinewood and mixed-pine peaks. This delay of peak super-pine aerosol concentrations is attributed to a lack of synergy between the lignocellulosic biomass constituents when devolatilized individually, compared to the synergy that is present in pinewood and mixed-pine. Hemicellulose is observed to devolatilize at an earlier test time and lower reaction environment temperature compared to individual cellulose and lignin. When the constituents are mixed, as in the mixed-pine and pinewood, the onset of hemicellulose devolatilization may promote earlier devolatilization of the other biomass constituents due to development of increased porosity and a corresponding increase of surface area for heat transfer.

3.6. Simulated pinewood aerosol emission factors and median size

$EF_{N,BP}$ and $EF_{M,BP}$ were determined for super-pine and mixed-pine, where the former was determined using individual constituent data and Eqns. (4) and (5), during pyrolysis. Size-resolved results for super-pine and mixed-pine are compared to those for pinewood in Fig. 7, and good shape and magnitude agreement is observed for super-pine and mixed-pine results with pinewood results. Similar to the individual constituent results that were shown in Fig. 4, ultra-fine aerosols dominated the number distribution while larger, accumulation-mode aerosols dominated the mass distribution. Table 3 summarizes $D_{50,N,BP}$ and $D_{50,M,BP}$ values for super-pine and mixed-pine, and the results compare very well with those of pinewood.

Super-pine and mixed-pine $EF_{N,tot,BP}$ and $EF_{M,tot,BP}$ are shown in Table 3 and compared to those of pinewood. Super-pine and mixed-pine $EF_{N,tot,BP}$ results agree with the pinewood result within 19% and 32%, respectively, and super-pine and mixed-pine $EF_{M,tot,BP}$ agree with the pinewood result within 4% and 23%, respectively. The mixed constituent sample (mixed-pine) had a reduced $EF_{N,tot,BP}$ and $EF_{M,tot,BP}$ compared to the superimposed individual constituent (super-pine) results. This suggests that gas-to-particle conversion of particle precursor species was reduced when products of pyrolysis included species from each constituent, compared to the higher partial pressures of particle precursor species having the same saturation pressure produced from individual constituent pyrolysis. Furthermore, the underprediction of pinewood $EF_{N,tot,BP}$ and $EF_{M,tot,BP}$ by mixed-pine may suggest that protein, extractive, and inorganic biomass contents contribute to aerosol formation during biomass pyrolysis. The additions and influences of such components could be tested in future work using the platform and approaches developed in this work, such as the preparation and testing of mixed constituent samples that include added inorganic content. Overall, super-pine and mixed-pine results both captured the aerosol formation behavior of pinewood well, and the results show that the superposition approach to modeling BB emissions based on those of individual constituents predicts biomass concentrations, median size, and emission factors comparably to mixed constituent samples and real biomass.

3.7. Simulated pinewood aerosol volatility

The MFR of the aerosol emissions was also determined for super-pine and mixed-pine at TD temperatures of 150 °C and 300 °C to investigate the predictability of biomass pyrolysis aerosol volatility based upon constituent performance and the mass fraction of each constituent in the biomass, and results are compared to pinewood in Fig. 8. MFR at a TD temperature of 150 °C was determined to be 0.076 ± 0.010, 0.084 ± 0.011, and 0.046 ± 0.024 for super-pine, mixed-pine, and pinewood, respectively, and the MFR was reduced to below 0.012 for each sample at 300 °C. Both super-pine and mixed-pine MFR results showed good agreement with pinewood at each tested TD temperature. The agreement of the results suggests that the volatility of biomass pyrolysis aerosols is significantly influenced by their lignocellulosic constituent composition, and that biomass pyrolysis aerosol volatility, in addition to aerosol concentrations,

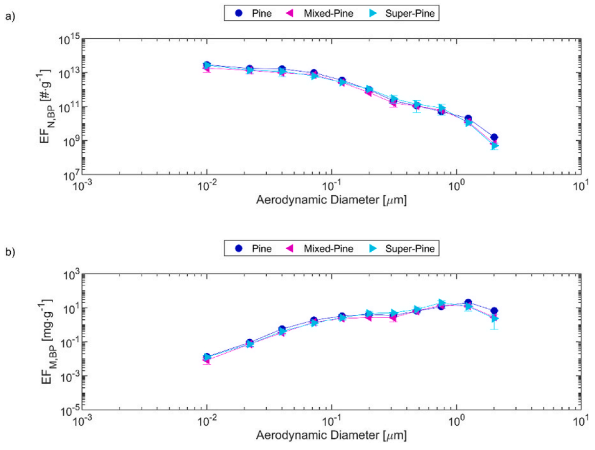

Fig. 7. Size-resolved a) number and b) mass aerosol emission factors determined for pyrolysis of super-pine, mixed-pine, and pinewood, where the bypass sample line was used for experimental measurements.

Table 3
Median aerosol number ($D_{50,N,BP}$) and mass ($D_{50,M,BP}$) diameters and total aerosol number ($EF_{N,tot,BP}$) and mass ($EF_{M,tot,BP}$) emission factors measured from pyrolysis of pinewood and mixed-pine, and simulated for pyrolysis of super-pine.

Pyrolysis	$D_{50,N}$ BP [μm]			$D_{50,M}$ BP [μm]			$EF_{N,tot}$ [$\#\cdot g^{-1}$]			$EF_{M,tot}$ [$mg\cdot g^{-1}$]		
	Avg.		Dev.	Avg.		Dev.	Avg.		Dev.	Avg.		Dev.
Pine	0.016	±	0.002	0.699	±	0.002	7.7E+13	±	7.5E+12	58.5	±	4.6
Mixed Pine	0.016	±	0.004	0.598	±	0.002	5.2E+13	±	9.5E+12	45.2	±	2.7
Superimposed Pine	0.013	±	0.003	0.55	±	0.088	6.2E+13	±	1.2E+13	55.7	±	8.9

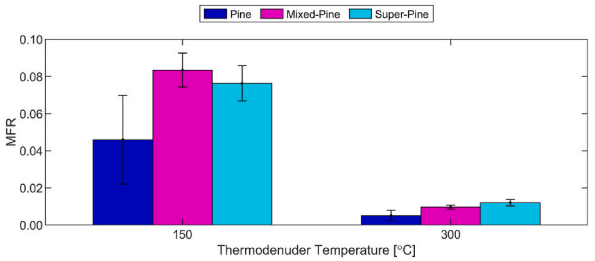

Fig. 8. Thermodenuded aerosol mass fraction remaining (MFR) from pyrolysis of super-pine and mixed-pine compared to pinewood. Two thermodenuder temperatures of 150 °C and 300 °C are shown.

median size, and emission factors, can be predicted via the superposition of constituent-derived results under the same pyrolysis conditions.

3.8. Influence of combustion on pinewood aerosol emissions

While this work focused on pinewood pyrolysis, additional tests were performed in which pinewood was heated in an air environment following the same procedure of the pyrolysis tests. These tests were performed in order to evaluate the applicability of pyrolysis tests, such as were the focus of this study, to understanding oxidation-derived aerosol emissions. Additionally, these tests allow for direct comparison of pyrolysis and oxidation aerosol emissions under the well-defined experimental conditions of this study,

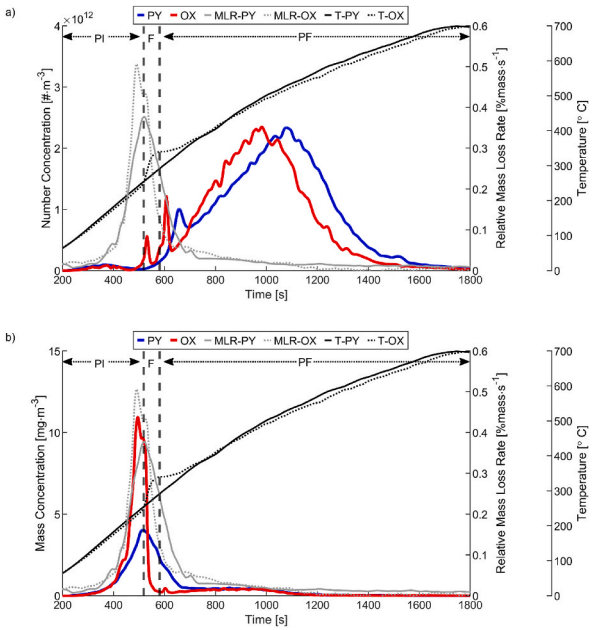

Fig. 9. Comparison of time-resolved pinewood pyrolysis (PY) and oxidation (OX) aerosol a) number concentration and b) mass concentration, determined using the bypass sample line. A representative relative mass loss rate (RMLR) is shown for each environment along with a representative gas environment temperature (T). Pre-ignition (PI), flaming (F), and post-flaming (PF) phases are denoted for the oxidative test with vertical dashed lines.

and elucidate influences of combustion on the aerosol emissions produced under the same set of heating and sampling conditions applied during pyrolysis in this work. Bypass pyrolysis and oxidation number and mass concentration data are shown in Fig. 9 along with a representative RMLR and gas environment temperature (T) for each environment. In the oxidative environment, pre-ignition pyrolysis (PI), flaming (F), and post-flaming smoldering (PF) burn phases were observed and the burn phases are denoted in Fig. 9. Each phase was distinguished by the onset and termination of visible flaming which could be observed through the macro-TGA quartz tube. A sharp increase and subsequent decrease of the reaction environment temperature is observed during flaming, and the total flaming phase lasted an average of 65 s. The peak RMLR observed over the oxidation test was 0.51 %mass·s^{-1}, and increased RMLR during oxidation compared to pyrolysis, which peaked at 0.38 %mass·s^{-1}, is attributable to accelerated fuel consumption in the presence of combustion and associated elevated gas temperatures. Number and mass concentration data were very similar in the pyrolysis and oxidative environments before ignition and flaming, and this result demonstrates that pinewood pyrolysis experimentation can offer insights into the significant fraction of BB emissions that occur prior to flaming in an oxidative environment. Following the onset of flaming combustion, aerosol mass concentration decreased sharply and remained low until flaming ceased, while number concentration initially increased upon flaming and then decreased. This finding aligns with work by Haslett et al. (Haslett et al., 2018) which showed that the onset of flaming sharply decreases the formation of organic aerosols. The onset of a significant number concentration in the oxidative environment at the start of post-flaming smoldering is observed at about 60 s earlier than a similar onset observed during pyrolysis tests, and this is attributed to an elevated reaction environment temperature in the oxidative environment. Apart from this temporal discrepancy, aerosol emissions are once again shown to be similar in number and mass between pyrolysis and oxidation in the time frame corresponding to post-flaming in the oxidative test.

Size-resolved and total number and mass emission factors were also determined over the duration of pinewood oxidation tests utilizing the bypass, and entire oxidation and individual burn phase results are presented in the Supplemental Material. $D_{50,N,BP}$ and $D_{50,M,BP}$ were determined to be 0.014 ± 0.001 μm and 0.845 ± 0.072 μm in the oxidative environment, and $D_{50,M,BP}$ results show that larger aerosols were measured in the oxidative environment compared to the pyrolysis environment (0.699 ± 0.002 μm). This result supports the suggested finding by McLaughlin & Belmont (McLaughlin & Belmont, 2021a) that influences of complex combustion reactions (Fitzpatrick et al., 2007; Orasche et al., 2013) and increased AMLR in oxidative environments lead to larger aerosol diameters compared to inert environments.

$EF_{N,tot,BP}$ and $EF_{M,tot,BP}$ were 5.1e13 ± 7.2e12 #·g^{-1} and 48.6 ± 8.3 mg·g^{-1} in the oxidative environment, respectively. $EF_{M,tot,BP}$ for pinewood oxidation measured in this study agrees well with mass emission factor ranges in the literature for pinewood burning, such as 7.5–62.5 g·kg^{-1} (Grandesso et al., 2011) and 7–77 g·kg^{-1} (Vose et al., 1996), suggesting suitability of the macro-TGA platform for measurement of aerosol emissions from representative fuels and under relevant conditions. $EF_{N,tot,BP}$ and $EF_{M,tot,BP}$ were reduced 34% and 17% from the pyrolysis to oxidative environments, respectively, and the result aligns with preceding work which showed average reductions of 51% and 37% for $EF_{N,tot,BP}$ and $EF_{M,tot,BP}$, respectively, between pyrolysis and oxidative environments (McLaughlin & Belmont, 2021a). The reaction environment dependencies are attributable to complex competing influences of combustion chemistry, including the consumption and alteration of particle precursor species via oxidation, and increased fuel AMLR in the oxidative environment increasing aerosol coagulation and growth (Fitzpatrick et al., 2007; Jöller et al., 2005; May et al., 2013; Orasche et al., 2013; Sakamoto et al., 2016).

Finally, the mass fraction remaining (MFR) of aerosols in the emissions stream as a function of TD temperature was compared between pinewood pyrolysis and oxidation tests to investigate the influence of burning conditions on the volatility of BB-derived aerosols, and results are presented in the Supplemental Material. MFR decreased with increased TD temperature for both pyrolysis and oxidation, as expected. The thermodenuder temperature corresponding to a 50% MFR, $T_{TD,50}$, was 54 °C and 59 °C for pyrolysis and oxidation, respectively, indicating that less volatile aerosols were formed in the oxidative environment. $T_{TD,50}$ for pinewood oxidation measured in this study compares well with that reported by Huffman et al. (Huffman, Docherty, Mohr, et al., 2009) for lodgepole pinewood burning ($T_{TD,50}$ of 61 °C) and that by Grieshop et al. (Grieshop, Logue, Donahue, & Robinson, 2009) for woodstove BB organic aerosols ($T_{TD,50}$ of 42 °C) within 4% and 29%, respectively. The MFR for pinewood pyrolysis was reduced by an average of 43% compared to the MFR for pinewood oxidation. This result is attributed to combustion reactions altering the chemical composition of particle precursor species, producing less OA and more BC and elemental carbon (EC) in oxidative environments, notably during flaming combustion, compared to pure pyrolysis.

Together, this comparison of pyrolysis and oxidation results highlights the similarity of pyrolysis emissions in each reaction environment, supporting the use of pyrolysis experimentation in a hierarchical approach to developing aerosol prediction models which capture the many complex effects that influence BB emissions. Additionally, the results show the extent to which oxidation reduces aerosol number and mass emission factors, as well as aerosol volatility, under the well-defined heating and sampling conditions in this work.

4. Conclusions

This study characterized primary aerosol emissions from pyrolysis of biomass and major lignocellulosic constituents under well-characterized conditions using a readily modeled macro-TGA platform. The work also evaluated a simple superposition model to test a hypothesis that primary biomass pyrolysis aerosol emissions can be predicted from lignocellulosic composition and the aerosol emissions of the three major constituents of lignocellulosic biomass when those constituents are exposed to the same conditions as the biomass itself. The superposition model was applied to test aerosol concentrations, size, emission factors, and volatility against those of pinewood biomass. Additionally, major lignocellulosic constituents were mixed in proportions equal to their proportions in pine to

create an experimentally simulated "pine" (mixed-pine), and pyrolysis of mixed-pine was conducted to evaluate any synergistic effects of constituent pyrolysis, as well as guide future investigations into the effects of constituents that were not considered in this work. Biomass and constituent samples were pyrolyzed using a macro-TGA, and aerosol concentrations, emission factors, median diameters, and volatility were determined using a cascade impactor and thermodenuder. The results showed that cellulose and lignin contribute strongly to aerosol size and quantity, and lignin decreases aerosol volatility while cellulose and hemicellulose increase aerosol volatility. Aerosols produced from the pyrolysis of pinewood were compared to those from the superposition model (super-pine) and mixed-pine, with all results showing favorable agreement. Synergistic effects between constituents in mixed-pine were shown to promote fuel devolatilization at lower reaction temperatures, similar to real pinewood, and this effect was not captured in super-position modeling. An additional important distinction was that mixed-pine samples produced lower total number and mass emission factors compared to super-pine results, and the finding suggests that the gas-to-particle conversion of pyrolysis products from mixed constituent samples is reduced compared to products from individual constituent samples, for which the partial pressure of particle precursor species having the same saturation pressure is increased. Lastly, the influence of combustion on the pinewood aerosol emissions and a comparison to pyrolysis was introduced. Pre- and post-flaming pyrolysis aerosols in an air environment were similar to those in an inert environment, but combustion in an oxidative environment was shown to overall reduce aerosol number and mass emission factors, as well as volatility. These tests highlighted similarities and differences between pyrolysis and oxidation emissions under similar conditions and the utility of studying pyrolysis emissions in order to understand oxidation-derived emissions.

Overall, the super-pine and mixed-pine results agreed well with pinewood concentrations, emission factors, size, and volatility, and the ability to predict primary biomass pyrolysis aerosol emissions based on lignocellulosic composition and constituent emissions was demonstrated. The agreement of modeled and measured emissions in this work invites future work to use the results of this study to validate hierarchical models and submodels of aerosol formation from biomass burning. Furthermore, the superposition model and mixed constituent approach used in this work can be readily expanded to test influences of other biomass content, such as inorganic content, on aerosol formation. Additionally, the techniques that were developed and demonstrated in this work provide a well-defined platform that can be used to explore aerosol emissions production under other conditions, such as for different fuel types, fuel conditioning, reaction environment, heating, and dilution conditions, and generate additional insights for aerosol model development and validation.

Funding sources

This work was supported by the National Science Foundation Graduate Research Fellowship Award #2137426 and the National Science Foundation Award #1847498.

Declaration of competing interest

The authors declare that they have no known competing financial interests or personal relationships that could have appeared to influence the work reported in this paper.

Acknowledgments

The contributions of Dr. Ed Wolfrum from the National Renewable Energy Laboratory (NREL) in Golden, CO to this work are gratefully acknowledged here.

Appendix A. Supplementary data

Supplementary data to this article can be found online at https://doi.org/10.1016/j.jaerosci.2022.106067.

References

An, W. J., Pathak, R. K., Lee, B. H., & Pandis, S. N. (2007). Aerosol volatility measurement using an improved thermodenuder: Application to secondary organic aerosol. *Journal of Aerosol Science, 38*(3), 305–314. https://doi.org/10.1016/j.jaerosci.2006.12.002

Bond, T. C., Streets, D. G., Yarber, K. F., Nelson, S. M., Woo, J. H., & Klimont, Z. (2004). A technology-based global inventory of black and organic carbon emissions from combustion. *Journal of Geophysical Research: Atmospheres, 109*(14), 1–43. https://doi.org/10.1029/2003JD003697

Cai, J., He, Y., Yu, X., Banks, S. W., Yang, Y., Zhang, X., et al. (2017). Review of physicochemical properties and analytical characterization of lignocellulosic biomass. *Renewable and Sustainable Energy Reviews, 76*, 309–322. https://doi.org/10.1016/j.rser.2017.03.072

Collier, S., Zhou, S., Onasch, T. B., Jaffe, D. A., Kleinman, L., Sedlacek, A. J., et al. (2016). Regional influence of aerosol emissions from wildfires driven by combustion efficiency: Insights from the BBOP campaign. *Environmental Science and Technology, 50*(16), 8613–8622. https://doi.org/10.1021/acs.est.6b01617

Di Blasi, C., Branca, C., Santoro, A., & Gonzalez Hernandez, E. (2001). Pyrolytic behavior and products of some wood varieties. *Combustion and Flame, 124*(1–2), 165–177. https://doi.org/10.1016/S0010-2180(00)00191-7

Evans, R. J., & Milne, T. A. (1987). Molecular characterization of the pyrolysis of biomass. *Energy and Fuels, 1*(2), 123–137. https://doi.org/10.1021/ef00002a001

Fachinger, F., Drewnick, F., Gieré, R., & Borrmann, S. (2017). How the user can influence particulate emissions from residential wood and pellet stoves: Emission factors for different fuels and burning conditions. *Atmospheric Environment, 158*, 216–226. https://doi.org/10.1016/j.atmosenv.2017.03.027

Faulhaber, A. E., Thomas, B. M., Jimenez, J. L., Jayne, J. T., Worsnop, D. R., & Ziemann, P. J. (2009). Characterization of a thermodenuder-particle beam mass spectrometer system for the study of organic aerosol volatility and composition. *Atmospheric Measurement Techniques, 2*(1), 15–31. https://doi.org/10.5194/amt-2-15-2009

Fawaz, M., Avery, A., Onasch, T. B., Williams, L. R., & Bond, T. C. (2021). Technical note: Pyrolysis principles explain time-resolved organic aerosol release from biomass burning. *Atmospheric Chemistry and Physics, 21*(20), 15605–15618. https://doi.org/10.5194/acp-21-15605-2021

Fitzpatrick, E. M., Ross, A. B., Bates, J., Andrews, G., Jones, J. M., Phylaktou, H., et al. (2007). Emission of oxygenated species from the combustion of pine wood and its relation to soot formation. *Process Safety and Environmental Protection, 85*(5 B), 430–440. https://doi.org/10.1205/psep07020

Grandesso, E., Gullett, B., Touati, A., & Tabor, D. (2011). Effect of moisture, charge size, and chlorine concentration on PCDD/F emissions from simulated open burning of forest biomass. *Environmental Science and Technology, 45*(9), 3887–3894. https://doi.org/10.1021/es103686t

Grieshop, A. P., Logue, J. M., Donahue, N. M., & Robinson, A. L. (2009). Laboratory investigation of photochemical oxidation of organic aerosol from wood fires 1: Measurement and simulation of organic aerosol evolution. *Atmospheric Chemistry and Physics, 9*(4), 1263–1277. https://doi.org/10.5194/acp-9-1263-2009

Grønli, M. G., Várhegyi, G., & Di Blasi, C. (2002). Thermogravimetric analysis and devolatilization kinetics of wood. *Industrial & Engineering Chemistry Research, 41*(17), 4201–4208. https://doi.org/10.1021/ie0201157

Haslett, S. L., Thomas, J. C., Morgan, W. T., Hadden, R., Liu, D., Allan, J. D., et al. (2018). Highly controlled, reproducible measurements of aerosol emissions from combustion of a common African biofuel source. *Atmospheric Chemistry and Physics, 18*(1), 385–403. https://doi.org/10.5194/acp-18-385-2018

Hays, M. D., Geron, C. D., Linna, K. J., Smith, N. D., & Schauer, J. J. (2002). Speciation of gas-phase and fine particle emissions from burning of foliar fuels. *Environmental Science and Technology, 36*(11), 2281–2295. https://doi.org/10.1021/es0111683

Huffman, J. A., Docherty, K. S., Aiken, A. C., Cubison, M. J., Ulbrich, I. M., Decarlo, P. F., et al. (2009). Chemically-resolved aerosol volatility measurements from two megacity field studies. *Atmospheric Chemistry and Physics, 9*(18), 7161–7182. https://doi.org/10.5194/acp-9-7161-2009

Huffman, J. A., Docherty, K. S., Mohr, C., Cubison, M. J., Ulbrich, I. M., Ziemann, P. J., et al. (2009). Chemically-resolved volatility measurements of organic aerosol from different sources. *Environmental Science and Technology, 43*(14), 5351–5357. https://doi.org/10.1021/es803539d

Iisa, K., Johansson, A. C., Pettersson, E., French, R. J., Orton, K. A., & Wiinikka, H. (2019). Chemical and physical characterization of aerosols from fast pyrolysis of biomass. *Journal of Analytical and Applied Pyrolysis, 142*, Article 104606. https://doi.org/10.1016/j.jaap.2019.04.022

Jöller, M., Brunner, T., & Obernberger, I. (2005). Modeling of aerosol formation during biomass combustion in grate furnaces and comparison with measurements. *Energy and Fuels, 19*(1), 311–323. https://doi.org/10.1021/ef049904m

Jolleys, M. D., Coe, H., McFiggans, G., McMeeking, G. R., Lee, T., Kreidenweis, S. M., et al. (2014). Organic aerosol emission ratios from the laboratory combustion of biomass fuels. *Journal of Geophysical Research: Atmospheres*, 850–871. https://doi.org/10.1002/2014JD021589.Received

López-García, M., Lodeiro, P., Herrero, R., Barriada, J. L., Rey-Castro, C., David, C., et al. (2013). Experimental evidences for a new model in the description of the adsorption-coupled reduction of Cr(VI) by protonated banana skin. *Bioresource Technology, 139*, 181–189. https://doi.org/10.1016/j.biortech.2013.04.044

May, A. A., Levin, E. J. T., Hennigan, C. J., Riipinen, I., Lee, T., Collett, J. L., et al. (2013). Gas-particle partitioning of primary organic aerosol emissions: 3. Biomass burning. *Journal of Geophysical Research: Atmospheres, 118*(19). https://doi.org/10.1002/jgrd.50828, 11,327-11,338.

May, A. A., McMeeking, G. R., Lee, T., Taylor, J. W., Craven, J. S., Burling, I., et al. (2014). Aerosol emissions from prescribed fires in the United States: A synthesis of laboratory and aircraft measurements. *Journal of Geophysical Research, 3*, 180–198. https://doi.org/10.1002/2014JD021848.Received

McLaughlin, L. P. (2022). Characterization of lignocellulosic biomass and constituent burning aerosols [university of Wyoming PP - United States – Wyoming]. In *ProQuest dissertations and theses*. https://www.libproxy.uwyo.edu/login?url=https://www.proquest.com/dissertations-theses/characterization-lignocellulosic-biomass/docview/2676913277/se-2?accountid=14793.

McLaughlin, L. P., & Belmont, E. L. (2021a). Impacts of oxidizer concentration and fuel composition on near-source aerosol emissions from lignocellulosic biomass and constituent burning. *Journal of Aerosol Science, 158*, Article 105825. https://doi.org/10.1016/j.jaerosci.2021.105825

McLaughlin, L. P., & Belmont, E. L. (2021b). Size-resolved aerosol emissions from lignocellulosic biomass and biomass constituent pyrolysis under variable dilution temperatures. *Journal of Aerosol Science, 151*, Article 105679. https://doi.org/10.1016/j.jaerosci.2020.105679

Mitchell, E. J. S., Lea-langton, A. R., Jones, J. M., Williams, A., Layden, P., & Johnson, R. (2016). The impact of fuel properties on the emissions from the combustion of biomass and other solid fuels in a fi xed bed domestic stove. *Fuel Processing Technology, 142*, 115–123. https://doi.org/10.1016/j.fuproc.2015.09.031

Morf, P., Hasler, P., & Nussbaumer, T. (2002). Mechanisms and kinetics of homogeneous secondary reactions of tar from continuous pyrolysis of wood chips. *Fuel, 81*(7), 843–853. https://doi.org/10.1016/S0016-2361(01)00216-2

Nielsen, I. E., Eriksson, A. C., Lindgren, R., Martinsson, J., Nyström, R., Nordin, E. Z., et al. (2017). Time-resolved analysis of particle emissions from residential biomass combustion – emissions of refractory black carbon, PAHs and organic tracers. *Atmospheric Environment, 165*, 179–190. https://doi.org/10.1016/j.atmosenv.2017.06.033

Orasche, J., Schnelle-Kreis, J., Schön, C., Hartmann, H., Ruppert, H., Arteaga-Salas, J. M., et al. (2013). Comparison of emissions from wood combustion. Part 2: Impact of combustion conditions on emission factors and characteristics of particle-bound organic species and polycyclic aromatic hydrocarbon (PAH)-related toxicological potential. *Energy and Fuels, 27*(3), 1482–1491. https://doi.org/10.1021/ef301506h

Reid, J. S., Koppmann, R., Eck, T. F., & Eleuterio, D. P. (2005). A review of biomass burning emissions part II : Intensive physical properties of biomass burning particles. *Atmospheric Chemistry and Physics, 5*, 799–825. https://doi.org/10.5194/acp-5-799-2005

Sakamoto, K. M., Laing, J. R., Stevens, R. G., Jaffe, D. A., & Pierce, J. R. (2016). The evolution of biomass-burning aerosol size distributions due to coagulation: Dependence on fire and meteorological details and parameterization. *Atmospheric Chemistry and Physics, 16*(12), 7709–7724. https://doi.org/10.5194/acp-16-7709-2016

Shafizadeh, F. (1982). Introduction to pyrolysis of biomass. *Journal of Analytical and Applied Pyrolysis, 3*(4), 283–305. https://doi.org/10.1016/0165-2370(82)80017-X

Van Zyl, L., Tryner, J., Bilsback, K. R., Good, N., Hecobian, A., Sullivan, A., et al. (2019). Effects of fuel moisture content on emissions from a rocket-elbow cookstove. *Environmental Science and Technology, 53*(8), 4648–4656. https://doi.org/10.1021/acs.est.9b00235

Vassilev, S. V., Vassileva, C. G., Song, Y. C., Li, W. Y., & Feng, J. (2017). Ash contents and ash-forming elements of biomass and their significance for solid biofuel combustion. *Fuel*, 377–409. https://doi.org/10.1016/j.fuel.2017.07.036, 208.

Vose, J. M., Swank, W. T., Geron, C. D., & Major, A. E. (1996). Emissions from forest burning in the southeastern United States: Application of a model determining spatial and temporal fire variation. In *Biomass burning and global change volume 2 biomass burning in South America , Southeast Asia , and temperate and Boreal ecosystems , and the Oil Fires of Kuwait* (Vol. 2, pp. 733–749). The MIT Press.

Yang, W., Pudasainee, D., Gupta, R., Li, W., Wang, B., & Sun, L. (2021). An overview of inorganic particulate matter emission from coal/biomass/MSW combustion: Sampling and measurement, formation, distribution, inorganic composition and influencing factors. *Fuel Processing Technology, 213*, Article 106657. https://doi.org/10.1016/j.fuproc.2020.106657

Zhang, Y., Obrist, D., Zielinska, B., & Gertler, A. (2013). Particulate emissions from different types of biomass burning. *Atmospheric Environment, 72*, 27–35. https://doi.org/10.1016/j.atmosenv.2013.02.026